Proceedings of GT2006
ASME Turbo Expo 2006: Power for Land, Sea and Air
May 8-11, 2006, Barcelona, Spain

GT2006-90978

RESPONSE SURFACE-BASED TRANSITION DUCT SHAPE OPTIMIZATION

Fredrik Wallin*
Division of Fluid Dynamics
Department of Applied Mechanics
Chalmers University of Technology
SE-412 96 Göteborg, Sweden
Email: fredrik.wallin@chalmers.se

Lars-Erik Eriksson
Division of Fluid Dynamics
Department of Applied Mechanics
Chalmers University of Technology
SE-412 96 Göteborg, Sweden
Email: lee@chalmers.se

ABSTRACT

Demands on improved efficiency and reduced noise levels cause a strive toward very high by-pass ratio (BPR) turbo-fan engines resulting in large fans and small high-pressure-ratio cores. The trend of increasing the radial offset between low- and high-pressure systems has made the design of intermediate transition ducts an area of growing importance. Shape optimization techniques for turbo-machinery applications have become a powerful aero-design tool and thanks to the rapid development of computer technology, computational fluid dynamics (CFD) may be used for optimization purposes. Surrogate model-based optimization has in recent years become a good alternative to the gradient-based search algorithms. One well-known surrogate model-based approach is response surface methodology (RSM), which has been used in the present work. RSM used together with design of experiments (DOE) can be a very efficient and robust method for CFD-based optimization. Optimization of two different transition ducts has been performed and evaluated; one 2D axi-symmetric turbine duct and one 3D compressor duct. The optimization objective was to minimize the total pressure loss. For the turbine duct both a high-Re and a low-Re turbulence closure were evaluated. The influence of design space size on the turbine duct optimization was investigated and for the 3D compressor duct the effects of adding an outflow constraint were examined. It has been found that end-wall optimization has the potential to reduce duct losses significantly. An early rapid diffusion and a stream-wise curvature shift toward the outlet seem to be important mechanisms for reducing transition duct losses.

NOMENCLATURE

Roman

A	Area
b	Estimated regression coefficients
C_p	Static pressure coefficient, $C_p = \frac{P-\overline{P_{out}}}{\frac{1}{2}\overline{\rho_{out}}\overline{u_{out}}^2}$
$c_1, c_2, ..$	Design parameters modifying the mean line
$d_1, d_2, ..$	Design parameters modifying the height
h	Duct height
k	Number of design parameters
	Turbulence kinetic energy
L	Duct length
m	Approximate duct mean line
n	Number of candidate designs
p	Number of regression model coefficients
P	Static pressure
P_i	i^{th} basis function
P_0	Stagnation pressure
q	Constraint coefficient
r	Radial co-ordinate
R^2	Coefficient of multiple determination
SS_E	Residual sum of squares
SS_T	Total sum of squares
u	Velocity
x	Axial co-ordinate
x_i	i^{th} design parameter
y	Response function
$\hat{y}$	Estimated response
y^+	Dimensionless wall normal distance

*Address all correspondence to this author.

Greek

β	Regression coefficients
ε	Random error
	Turbulence dissipation rate
ζ	Loss coefficient, $\frac{\overline{\overline{P_{0,in}}}-\overline{\overline{P_{0,out}}}}{\frac{1}{2}\overline{\rho_{in}}\,\overline{u_{in}}^2}$
μ	Viscosity
ρ	Density

Subscripts

h	Hub (duct inner-wall)
s	Shroud (duct casing)
in	Inlet
out	Outlet

Superscripts

$*$	Modified
$-$	Area average
$=$	Mass flow-weighted average

Abbreviations

BPR	By-Pass Ratio
CFD	Computational Fluid Dynamics
DOE	Design of Experiments
FCCD	Face-Centered Composite Design
HPC	High-Pressure Compressor
HPT	High-Pressure Turbine
HRN	High-Reynolds Number
LPC	Low-Pressure Compressor
LPT	Low-Pressure Turbine
LRN	Low-Reynolds Number
RANS	Reynolds-Averaged Navier-Stokes
RSM	Response Surface Methodology
SQP	Sequential Quadratic Programming

INTRODUCTION

In multi-spool turbo-fan engines of today demands on improved efficiency and reduced noise levels lead to high by-pass ratios (BPR). These demands result in engines with large fans and small high-pressure-ratio cores leading to a significant radial difference between the low-pressure and the high-pressure systems. To connect the two systems intermediate transition ducts are needed. The trend in modern turbo-fan engine design is toward even higher BPR, which will lead to an increased radial offset between the low- and high-pressure systems, causing a need for more aggressive transition ducts. This strive toward higher BPR makes duct design increasingly important and the interest in robust and reliable optimization techniques is thus growing. Figure 1 shows the large annular S-shaped ducts used to connect the low- and high-pressure systems of a modern two-spool turbo-fan engine. One intermediate transition duct connects the low- and high-pressure compressors (LPC and HPC) and another one connects the high- and low-pressure turbines (HPT and LPT).

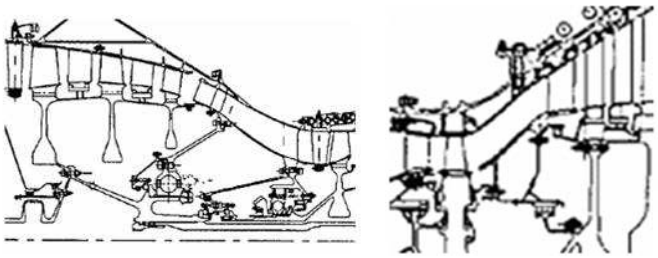

Figure 1. THE COMPRESSOR DUCT (LEFT) AND THE TURBINE DUCT (RIGHT) OF A HIGH BPR TURBO-FAN ENGINE.

The use of shape optimization within turbo-machinery design is possible today thanks to powerful computer resources for performing computational fluid dynamics (CFD) analysis. Surrogate model-based optimization has in recent years become a good alternative to the direct application of gradient-based search algorithms. It is a technique well suited for optimization involving costly CFD analysis. The basic idea of using surrogate models is to construct an approximation of the true goal-function (response) from a set of candidate designs (training data). One such well-known surrogate model-based approach is response surface methodology (RSM), which tends to be a robust and smooth optimization technique and thus insensitive to numerical noise. RSM is therefore commonly used for global optimization problems. Papila et al [1] used RSM for preliminary design optimization of a supersonic turbine and for further investigation of such turbines Papila et al [2] used a method combining radial basis neural networks with RSM. Madsen et al [3] used RSM for diffuser shape optimization and Unal et al [4] showed how suitable RSM is for use within multidisciplinary optimization. There are several other examples in the literature of surrogate model-based optimization for turbo-machinery applications.

In the present work the focus lie on intermediate transition duct end-wall shape optimization using CFD together with RSM. In using RSM, a design space is first defined and spanned by user-defined design parameters. A low number of candidate designs within the design space are chosen, according to the theory known as design of experiments (DOE). These designs constitute the training data from which a regression model can be constructed. The goal-function is evaluated for each of the designs using CFD and an approximation of the goal-function, a response surface, is constructed. In the present work second-order polynomial response surfaces are fitted to the training data. For a detailed description of DOE and RSM, the book by Myers and Montgomery [5] should be consulted.

PARAMETERIZATION

A major issue when using RSM is geometry parameterization. As the candidate designs have been evaluated a response surface is fitted to the obtained training data. When a second-order polynomial response surface is used, the number of regression coefficients (p) increases rapidly with the number of design parameters (k), according to the formula $p = (k+1)(k+2)/2$. This phenomena is sometimes referred to as the curse of dimensionality. As the number of regression model coefficients increases, so will the size of the candidate design set. The number of candidate designs (n) used to construct a regression model is $n \geq p$. Since every new design added to the training data set results in the need for one more CFD analysis, keeping the number of design parameters down is of great importance from an efficiency point of view. In order to keep the design parameters at a minimum, but still obtain maximum flexibility of our geometry an efficient way of modifying the original geometry is introduced. The idea is to apply perturbations to a reference duct. We know that there exists a perturbation such that it optimizes the duct geometry with respect to our defined goal-function. Hence an approximation to this perturbation is sought. A linear combination of basis functions is used to construct this approximate perturbation. To ensure that this approximation is the best possible, orthogonal polynomials (P_i) are used as basis functions. All polynomials are defined on the interval $0 \leq x \leq L$. Upstream components (LPC or HPT) and downstream components (HPC or LPT) often sets the duct inlet and outlet radius, flow angle and curvature. In order not to change the reference design conditions at inlet or outlet, the boundary conditions (1) are imposed on the orthogonal polynomials.

$$P_i(x) = \frac{dP_i}{dx} = \frac{d^2P_i}{dx^2} = 0 \text{ at } \begin{cases} x = 0 \\ x = L \end{cases} \tag{1}$$

The first basis function is defined as the lowest-order non-zero polynomial satisfying these boundary conditions. The basis functions are orthogonal to each other according to the norm (2).

$$\int_0^L P_i(x)\ P_j(x)\ dx \begin{cases} = 0 & \text{as } i \neq j \\ \neq 0 & \text{as } i = j \end{cases} \tag{2}$$

The next basis function is the lowest-order non-zero polynomial that satisfies the boundary conditions (1) and is orthogonal to all previously defined basis functions according to (2) and so on. Adopting this procedure results in the four first basis functions shown in figure 2. An infinite number of orthogonal polynomials can be defined, but in the present work only the two first polynomials (P_1 and P_2) have been used. The reference geometry is modified by adding (or subtracting) perturbations to functions

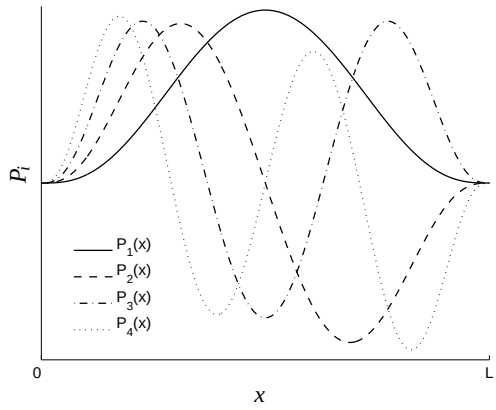

Figure 2. THE FOUR FIRST BASIS FUNCTIONS.

approximately corresponding to the duct mean line and the duct height distribution (measured form hub to shroud). These perturbations consist of linear combinations of the orthogonal polynomials defined. Having the mean line and height represent the duct geometry instead of the hub and shroud curves result in two functions with greater influence on and stronger coupling to the total duct design. The approximate mean line (m) and height (h) are defined by equation (3).

$$\begin{aligned} m(x) &= \frac{1}{2}r_s(x) + \frac{1}{2}r_h(x) \\ h(x) &= r_s(x) - r_h(x) \end{aligned} \tag{3}$$

Here r_h and r_s are the hub and shroud radii respectively. Commonly a duct geometry is described by defining its mean line and area distribution. In the present work the height distribution has been chosen over the area distribution to avoid the non-linearity associated with area calculations. To further simplify the parameterization, both functions describing the duct geometry (m and h) and also the basis functions (P_i) have been parameterized along the axial co-ordinate x. A parameterization along a stream-wise co-ordinate was considered, but would become less important as the number of basis functions is increased. Modifications to the reference geometry are done by assigning certain values to the design parameters c_i and d_i. These design parameters are then used as coefficients multiplying the basis functions. Equation (4) shows how the modified mean line (m^*) and height distribution (h^*) are calculated.

$$\begin{aligned} m^*(x) &= m(x) + \sum_{i=1}^{N} c_i P_i(x) \\ h^*(x) &= h(x) + \sum_{i=1}^{N} d_i P_i(x) \end{aligned} \tag{4}$$

N is here the number of basis functions used and thus the number of design parameters is $k = 2N$. The new duct geometry obtained, i. e. the modified hub (r_h^*) and shroud (r_s^*), is then described by equation (5).

$$r_h^*(x) = m^*(x) - \frac{1}{2}h^*(x)$$
$$r_s^*(x) = m^*(x) + \frac{1}{2}h^*(x) \quad (5)$$

DESIGN OF EXPERIMENTS

As mentioned earlier the number of regression model coefficients increases rapidly as the number of design parameters is increased. This in turn leads to an increased size of the training data set and thus more time-consuming CFD analyzes. In order to keep the size of the training data set at a minimum, a sound strategy for candidate design selection needs to be applied. This theory of choosing suitable designs for exploring the entire design space efficiently is known as the design of experiments (DOE). There are numerous different DOE approaches. In the present work a face-centered composite design (FCCD), which is a common method for fitting second-order models [6], has been used. The DOE procedure starts with a selection of design parameters to be used. These parameters will span the design space. The boundary of the design space is defined by the range chosen for each design parameter. A normalization of each design parameter is then performed so that the lower bounds of all design parameters correspond to the value -1 and the upper bounds correspond to +1. The candidate designs to be evaluated are given by the FCCD as all corners, all face-centers and the center point of the design space. This results in $n = 2^k + 2k + 1$ candidate designs. Figure 3 illustrates the FCCD strategy for a case of three design parameters (x_1, x_2 and x_3). It is not in the scope of this paper to investigate the benefits and drawbacks of different DOE methods.

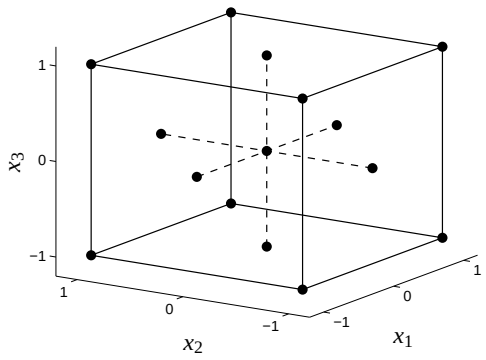

Figure 3. A THREE DESIGN PARAMETER FCCD.

FLOW SOLVER

An in-house compressible flow solver [7], has been used for all CFD analyzes. The code is based on a cell-centered finite-volume approach, adapted to a structured multi-block grid, to solve the governing compressible RANS equations. Third order upwinding is used for the convective flux and the upwinding biasing is based on local characteristic variables and speeds. A three-stage Runge-Kutta method is used for the time-marching. Turbulence is modeled using either a high-Re (HRN) or a low-Re (LRN) realizable k-ε closure.

In the present work standard wall-functions were used together with the HRN k-ε model [8]. The cell-centers adjacent to the walls were located at $y^+ \approx 30$ for the 2D calculations and at $y^+ \approx 25$ for the 3D analyzes. Chien's LRN k-ε model [9], was also used for the axi-symmetric turbine duct optimization. The 2D grids were refined in the wall-regions and a $y^+ \approx 1$ was obtained for all wall-adjacent cell-centers.

RESPONSE SURFACE METHODOLOGY

A regression model approximating the goal-function is constructed from the responses of the candidate designs chosen by the DOE method. In order to find these responses one CFD analysis is performed for each design of the candidate set. Response surface-based optimization makes it possible to do these computations in parallel, since all CFD analyzes are independent of each other. Thus it is feasible to distribute the candidate design analyzes on different processors, making this optimization technique a very efficient one. Since the number of candidate designs given by the FCCD is larger than the number of regression coefficients, the regression model is over-fitted. As a result of this over-fitting the RSM technique is robust toward noisy response functions [3]. In the present work a second-order response surface is used to approximate the goal-function. This type of model takes the form of equation (6).

$$y = \beta_0 + \sum_{i=1}^{k} \beta_i x_i + \sum_{i=1}^{k} \beta_{ii} x_i^2 + \sum_{i<}^{} \sum_{j=2}^{k} \beta_{ij} x_i x_j + \varepsilon \quad (6)$$

Where y is the response function, the β's are the regression coefficients, x_i is the i^{th} design parameter, ε is the random error and k is the number of design parameters. The fitted regression model takes the form of equation (7).

$$\hat{y} = b_0 + \sum_{i=1}^{k} b_i x_i + \sum_{i=1}^{k} b_{ii} x_i^2 + \sum_{i<}^{} \sum_{j=2}^{k} b_{ij} x_i x_j \quad (7)$$

Here $\hat{y}$ is the approximation of the goal-function obtained by a least-square fit of a second-order response surface to the

true goal-function y. The b's are thus the least-square estimators of the regression coefficients. As a measure of the quality of the response surface fit the coefficient of multiple determination R^2 is often used. It is defined by equation (8).

$$R^2 = 1 - \frac{SS_E}{SS_T} \tag{8}$$

SS_E is known as the residual sum of squares and SS_T as the total sum of squares. These are defined by equations (9) and (10) respectively.

$$SS_E = \sum_{i=1}^{n} (y_i - \hat{y}_i)^2 \tag{9}$$

$$SS_T = \sum_{i=1}^{n} (y_i - \overline{y})^2 \tag{10}$$

Here y_i is the calculated response of the i^{th} design of the candidate set, $\hat{y}_i$ is the response surface approximation to y_i and $\overline{y}$ is the mean value of all calculated responses. However because R^2 always increases with the order of the model, it is preferable to define an adjusted R^2 [3] [6]. This is done by scaling the SS_E and SS_T terms by their associated degrees of freedom, as equation (11) shows.

$$R^2_{adj} = 1 - \frac{SS_E/(n-p)}{SS_T/(n-1)} \tag{11}$$

Where n is the number of candidate designs given by the DOE and p is the number of regression coefficients. A value of $R^2_{adj} = 1.0$ would correspond to a perfect fit, i. e. the response surface model predicts the exact same response as the CFD analysis for each candidate design.

Once the response surface approximation of the goal-function is constructed finding its optimum (minimum or maximum) is a simple procedure. Since the response surface is an analytic function a low-cost gradient-based search algorithm can be used to find the optimum. In the present work a sequential quadratic programming (SQP) method is adopted to solve the optimization problem [10].

TEST CASES

Two different optimization cases have been studied. One 2D axi-symmetric turbine duct and one 3D compressor duct with eight struts. The total pressure loss coefficient (ζ) defined by equation (12) has been used as goal-function.

$$\zeta = \frac{\overline{\overline{P_{0,in}}} - \overline{\overline{P_{0,out}}}}{\frac{1}{2}\overline{\rho_{in}}\,\overline{u_{in}}^2} \tag{12}$$

Here $\overline{\overline{P_{0,in}}}$ and $\overline{\overline{P_{0,out}}}$ are the mass flow-weighted stagnation pressures at the inlet and outlet respectively. The aim of the optimization in the present work is to minimize the total pressure loss. Therefore the duct length is kept constant. In a preliminary design process a fixed pressure loss and a variable duct length could be an alternative optimization problem. Even a multi-objective optimization problem with the intention to minimize both loss and length could be considered. That is however not in the scope of this paper.

2D Axi-symmetric Turbine Duct

The baseline geometry is based on the inlet and outlet radii defined for the Chalmers turbine duct testing facility [11]. The purpose is to optimize the turbine transition duct geometry for minimum pressure loss. RSM was used together with steady 2D axi-symmetric CFD analyzes. The duct has an area ratio $A_{out}/A_{in} = 1.60$, a non-dimensional length $L/h_{in} = 4.55$ and an aspect ratio $(\overline{r_{out}} - \overline{r_{in}})/L = 0.41$. Turbine ducts are commonly classified using the diagram by Sovran and Klomp [12], developed for determining optimum geometries for rectilinear diffusers with annular cross-sections. Adopting this classification would reveal the investigated duct to be fairly aggressive.

A baseline duct was designed by defining a mean line and an area distribution using two fifth order polynomials. Four design parameters were used for optimization of the duct geometry. Two design parameters (c_1 and c_2) to modify the duct mean line and two other design parameters (d_1 and d_2) to modify the duct height according to equation (4). Equation (13) formulates the optimization problem.

$$\textit{minimize} \quad \zeta(c_1, c_2, d_1, d_2) \tag{13}$$

Optimization using both a HRN and a LRN k-ε turbulence model was performed. Two different design spaces were also investigated. Design space I was chosen to be very large, including some extreme and somewhat unrealistic duct designs with severe separation. Design space II was set to be $1/16$-th of design space I by using only half the span of each design parameter. This results in a design space containing less extreme geometries, but it still covers a large variety of designs. The resulting optimum geometries for both design spaces investigated are shown in figure 4. For design space II only the optimum design obtained

by the HRN model is plotted, since it was very similar to the LRN model geometry obtained. The maximum radial difference between these two designs was less than 1.0 mm and the mean difference less than 0.5 mm. As a measure of the quality of the response surface fit the adjusted coefficients of multiple determination (R^2_{adj}) were calculated for each response surface and are presented in table 1.

Table 1. THE R^2_{adj} STATISTICS FOR THE TURBINE DUCT RESPONSE SURFACES.

	HRN model	LRN model
Design space I	0.948	0.949
Design space II	0.933	0.939

The loss coefficients predicted by the different models for the baseline and for the optimum ducts found are presented in table 2. Noticeable is that the choice of a large design space (design space I) in this case results in poor loss predictions for some of the extreme duct geometries evaluated when the HRN model with wall-functions is used. This will lead to a more unreliable regression model than the one obtained with the LRN model, although the R^2_{adj} statistics suggest that the quality of the fit of both models is about equal.

Table 2. LOSS PREDICTIONS (ζ) FOR THE TURBINE DUCT DESIGNS.

	HRN model		LRN model	
	RSM	CFD	RSM	CFD
Baseline	-	0.054	-	0.056
Design space I	0.038	0.045	0.047	0.047
Design space II	0.043	0.044	0.047	0.047

From figure 4 it can be seen that the two predicted optimum geometries are similar for design space I, using the HRN and the LRN models respectively, but table 2 reveals that the loss predicted from the HRN model response surface is off by almost 20% compared to CFD predictions for the optimum geometry. When the design space size is reduced (design space II), the loss prediction using the HRN model is greatly improved and shows quite good agreement with the direct CFD prediction. The LRN model response surfaces show very good agreement with the loss coefficient obtained from CFD analyzes of the optimum geometries for both design spaces evaluated. The similarity between the optimum geometries predicted by the HRN and the LRN model analyzes could be explained by the fact that the flow is 2-dimensional and non-separating though the duct is fairly aggressive. For a more aggressive duct, where the flow of the optimum design is closer to separation, larger differences would be expected.

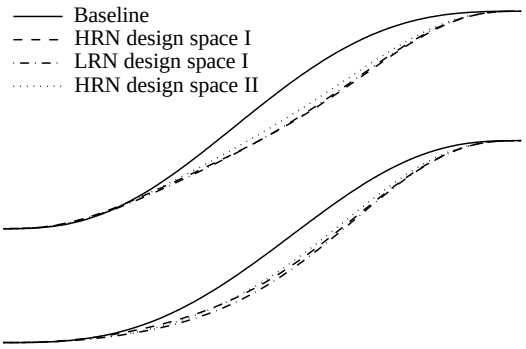

Figure 4. THE 2D AXI-SYMMETRIC TURBINE DUCT GEOMETRIES.

Results for design space II indicate a decrease in total pressure loss of about 19% for the HRN model calculations and about 16% for the LRN model analysis. The obtained levels of loss reduction are however not of major importance in the present study. In a real-life turbo-fan engine the flow into the turbine duct is greatly influenced by the upstream HPT. Incoming wakes and radial distortion is neglected in the 2D analysis performed here. No constraints on the geometry nor on any flow parameters have been considered either. However the results indicate that a significant loss reduction is possible to obtain by the use of shape optimization in the design process. The optimized designs also indicate some important mechanisms for reducing the duct losses. It can be seen in figure 5 that the mean line curvature is shifted toward the exit of the duct. The stream-wise area distribution, shown in figure 6, is also changed. This results in a larger diffusion in the first half of the duct. Thereby an area decrease in the middle of the duct is possible and thus a flow accelaration in the part of the duct were separation is most likely to occur.

3D Compressor Duct

The axi-symmetric shape of the end-walls of a compressor transition duct containing eight struts has been optimized for minimum pressure loss. Steady 3D CFD analyzes were used together with RSM. Turbulence was modeled using a HRN realizable k-ε closure with standard wall-functions. The baseline duct was designed by Rolls-Royce UK and is being installed in

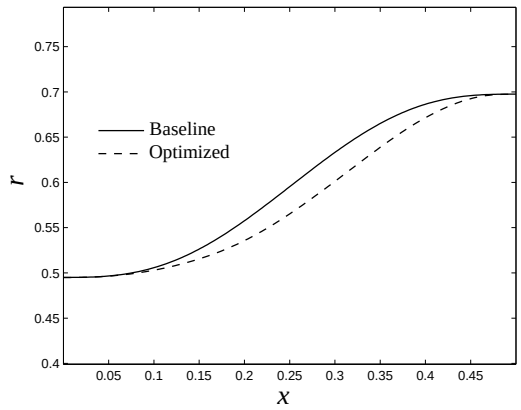

Figure 5. MEAN LINE OF THE BASELINE AND OPTIMIZED TURBINE DUCTS.

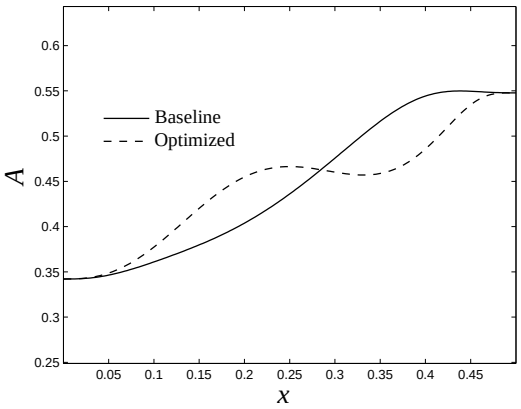

Figure 6. AREA DISTRIBUTION OF THE BASELINE AND OPTIMIZED TURBINE DUCTS.

a test facility at Loughbourough University. An inlet boundary condition profile was also provided by Rolls-Royce UK. In using this radial inlet profile some of the effects from upstream components are taken into account. A passage between two struts of the baseline duct is shown along with the surface mesh used for CFD analysis in figure 7. The eight struts cause a blockage of almost 25% when compared to the clean baseline duct (without struts). The duct has an area ratio $A_{out}/A_{in} = 1.00$ and a non-dimensional length $L/h_{in} = 3.33$. The strut geometry was defined from hub to shroud of the baseline duct. A linear extrapolation of this original strut geometry was performed to ensure that all modified duct designs investigated would have the strut reaching outside their end-walls. Then for each individual design the strut was cut off at the hub and shroud surfaces to fit inside that specific duct.

As in the 2D axi-symmetric optimization study four design parameters have been used and the optimization problem is described by equation (13). The design parameters c_1 and c_2 modify the approximate mean line and d_1 and d_2 perturb the height

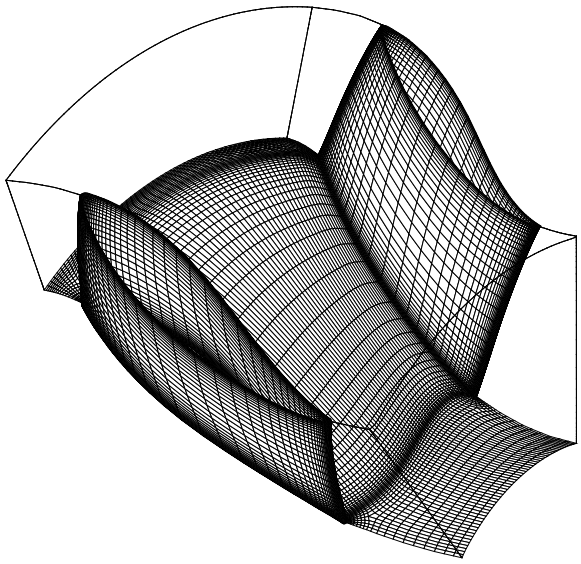

Figure 7. SURFACE MESH OF THE BASELINE COMPRESSOR DUCT.

distribution as described by equation (4). The 4-dimensional design space setup for the 3D optimization contains a large variety of designs. It is however clear from the loss predictions in table 3 and the response surface quality of fit statistic $R^2_{adj} = 0.998$ that it is a design space small enough to avoid unrealistic designs with large separations. This is desirable since separating flows could cause problems when using a HRN turbulence model with wall-functions, as observed in the 2D turbine duct optimization process. When comparing RSM and CFD loss coefficient predictions for the 3D case they show good agreement.

Table 3. LOSS PREDICTIONS (ζ) FOR THE COMPRESSOR DUCT DESIGNS.

	RSM	CFD
Baseline	-	0.079
Optimized	0.060	0.060

The resulting optimum duct design is compared to the baseline duct in figure 8. It is clear that the most significant difference between the optimized and the baseline ducts is the large increase of the stream-wise area distribution where the struts cause the largest blockage. A total pressure loss reduction of about 24% was achieved by optimization. As for the 2D axi-symmetric turbine duct analysis, the actual level of loss reduction obtained is not of major importance here since the effects a re-design would have on the downstream components are neglected. In order to

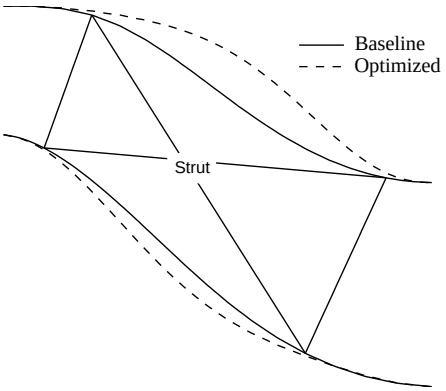

Figure 8. THE BASELINE VS. THE OPTIMIZED COMPRESSOR DUCT.

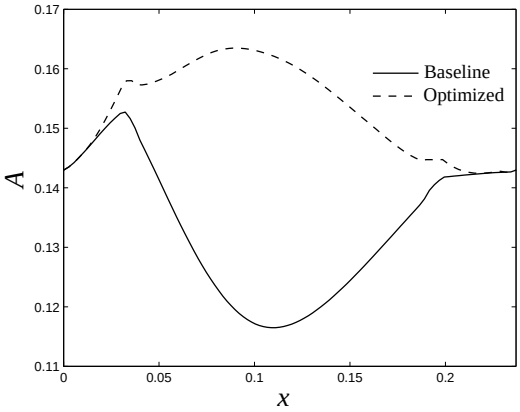

Figure 10. AREA DISTRIBUTION OF THE BASELINE AND OPTIMIZED COMPRESSOR DUCTS.

obtain more reasonable levels of achievable loss reduction some kind of geometry or outflow constraint is probably necessary. The results do however show the possible benefits of including shape optimization in the transition duct design process.

As in the turbine duct case previously presented, the optimized design also indicate some important mechanisms for decreasing losses. In figure 9 the mean lines of the baseline and optimized ducts are compared. A distinct shifting of stream-wise curvature toward the outlet of the optimized design is observed. This phenomena was also seen for the optimized turbine duct. A significant change of the area distribution is also observed from figure 10. The optimized duct opens up to compensate for the blockage caused by the struts. An early rapid diffusion is obtained and thereby an area decrease starting in the middle of the duct. The same tendency was observed in the turbine duct case. For the compressor duct this will result in a flow acceleration through the entire second half of the duct.

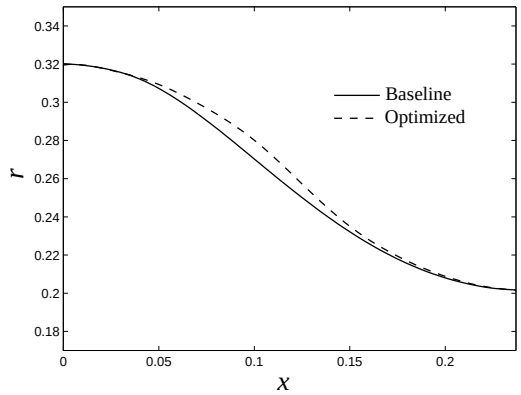

Figure 9. MEAN LINE OF THE BASELINE AND OPTIMIZED COMPRESSOR DUCTS.

Having eight thick struts in the duct results in wakes traveling downstream, causing major losses. From calculations done on the clean baseline duct a loss coefficient $\zeta = 0.040$ was predicted. Comparing this to $\zeta = 0.079$ for the same duct with struts shows that the loss is almost doubled, which illustrates the great impact the presence of struts has on the overall loss. An interesting observation is that the optimization has significant effects on the wake behavior. Figure 11 shows entropy contours at the duct outlet for the baseline and optimized ducts. The wake at the baseline duct outlet is thicker and deeper than the one at the optimized duct outlet. It is also highly twisted at the hub. The boundary layers are also thicker at the baseline duct outlet and seem to be more distorted.

Constrained Optimization

In the previous sections the unconstrained optimization of a 2D axi-symmetric turbine duct and a 3D compressor duct have been described. The focus of optimization was to minimize the total pressure loss by only modifying the duct end-walls. The effects on the outflow profile of changing the duct shape were neglected. In doing so the change of the inlet flow to any downstream component was not taken into consideration. However it has been shown that a significant reduction of the duct losses is possible to achieve by optimization of the shape of the duct end-walls. To address the issue of downstream effects, a constraint on the outflow profile should be added to the optimization problem. There are several possible ways to formulate such constraints. In the present work a limit on the deviation from the hub to shroud static pressure difference of the baseline duct ($\Delta P = P_{h,out} - P_{s,out}$) has been used as a constraint. Adding this constraint to the previously presented unconstrained optimization problem (13) results in the constrained problem formulated by equation (14).

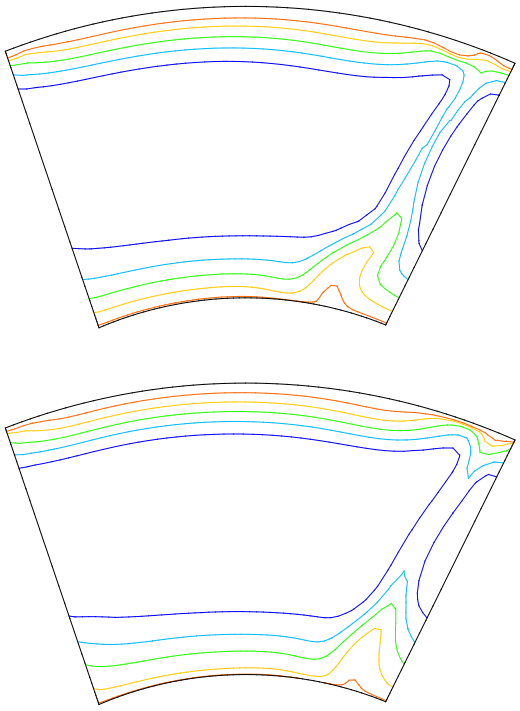

Figure 11. OUTLET ENTROPY CONTOURS OF THE BASELINE DUCT (TOP) AND OPTIMIZED DUCT (BOTTOM).

$$\begin{aligned} &\textit{minimize} \quad \zeta(c_1, c_2, d_1, d_2) \\ &\textit{subject to} \\ &\quad (1-q)\Delta P \leq \Delta P^*(c_1, c_2, d_1, d_2) \leq (1+q)\Delta P \end{aligned} \tag{14}$$

Here ΔP and ΔP^* are the circumferential averages of the hub to shroud static pressure difference of the baseline and optimized ducts respectively. q is the fraction of ΔP by which ΔP^* is allowed to differ. The results of the constrained 3D compressor duct optimization using two different values of q are presented. Figure 12 shows the optimized geometries using $q = 10\%$ and $q = 20\%$ compared both to the baseline duct and the duct obtained from the unconstrained optimization described in the previous section. This comparison clearly shows the great influence of an outflow constraint on the optimized duct geometry.

The effect of the applied constraint on the outflow pressure profile is visualized in figure 13. Here the static pressure coefficient (15) is plotted at the outlet of the four designs presented in figure 12.

$$C_p = \frac{P - \overline{P_{out}}}{\frac{1}{2}\overline{\rho_{out}}\,\overline{u_{out}}^2} \tag{15}$$

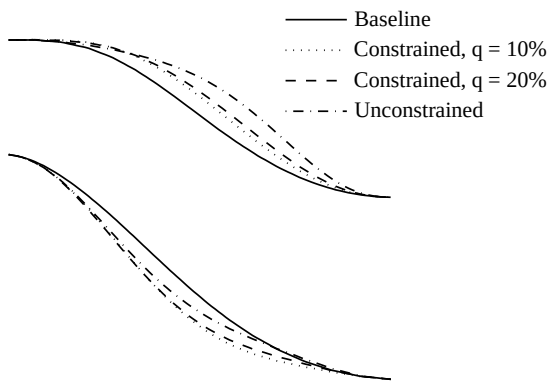

Figure 12. THE BASELINE VS. THE OPTIMIZED COMPRESSOR DUCTS OBTAINED USING AN OUTFLOW CONSTRAINT.

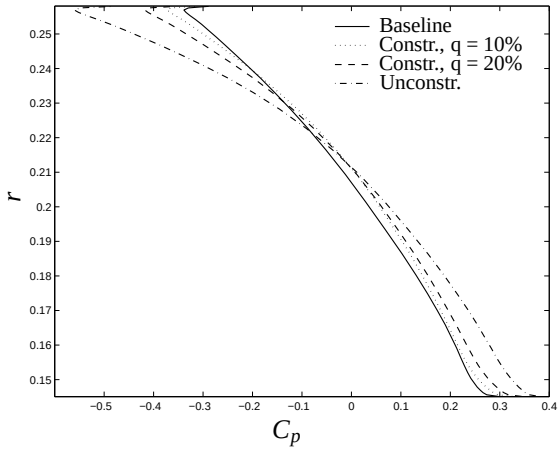

Figure 13. THE OUTFLOW PRESSURE PROFILES OF THE BASELINE AND THE OPTIMIZED COMPRESSOR DUCTS.

Restrictions on the outflow profile will exclude some optimal designs allowed in the unconstrained optimization. Thus the use of this constraint will affect the possible loss reduction obtained by optimization. In table 4 the predicted loss coefficients of the designs obtained from the constrained optimization are presented. Changes of the duct mean line curvature are clearly limited by the constraint. However it can be concluded that by focusing mainly on modifying the area distribution, a loss reduction of up to 16% may be obtained without changing the outlet hub to shroud static pressure difference by more than 10%. If an outlet static pressure difference of 20% is allowed a loss reduction of up to 20% can be obtained.

CONCLUSIONS

For aero-design of turbo-machinery applications using DOE and RSM together seems to be a suitable approach for finding optimum designs and exploring the design space and deciding

Table 4. LOSS PREDICTIONS (ζ) FOR THE CONSTRAINED OPTIMIZATION DUCT DESIGNS.

	RSM	CFD
Constrained, $q = 10\%$	0.065	0.066
Constrained, $q = 20\%$	0.062	0.063

on regions of acceptable designs. Thanks to the use of RSM the handling of goal-functions and constraints is straightforward. The method has the advantage of being suitable for parallel computing and requires a minimum of interfacing with other software such as mesh generator, CFD code and post-processor. Since orthogonal polynomials are used to modify the baseline duct shape, a wide variety of designs are possible to produce by only introducing a low number of design parameters. The idea of applying perturbations to a reference design is particularly attractive for re-design purposes.

Significant loss reduction may be obtained if shape optimization is included in the duct design process. Some of the mechanisms for decreasing duct losses are indicated by studying the resulting optimum designs presented. The turbine and compressor optimum designs show similar trends. A rapid diffusion in the beginning of both ducts makes an area decrease in the middle of the ducts possible. Thereby an acceleration of the flow is obtained in the area where boundary layer separation is most likely to occur. A shift of the strong stream-wise curvature toward the outlet reduces losses within the duct, but might affect the inflow to downstream components in a negative way. This was investigated by introducing an outflow constraint in the 3D compressor duct optimization. It was concluded that by considering an outlet profile restriction in this way the re-distribution of stream-wise curvature is limited. However even with this constraint active a significant loss reduction was obtained by primarily changing the duct area distribution.

The comparison between optimization using HRN and LRN turbulence modeling, show that although the two models predict quite different loss levels they produce similar optimum duct geometries. However this result may not be applicable to more aggressive duct optimization problems involving more realistic 3D CFD analysis and/or different goal-functions. The investigation of two different design spaces shows that using a larger design space results in a less accurate response surface model. Still a reasonable duct geometry can be obtained and used as a first step toward an optimum design.

ACKNOWLEDGMENT

The presented work was conducted within the EU Sixth Framework Project AIDA (Aggressive Intermediate Duct Aerodynamics for Competitive and Environmentally Friendly Jet Engines), contract number: AST3-CT-2003-502836.

REFERENCES

[1] Papila, N., Shyy, W., Griffin, L., Huber, F., and Tran, K., July, 2000. "Preliminary Design Optimization for a Supersonic Turbine for Rocket Propulsion". 36th AIAA/ASME/SAE/ASEE Joint Propulsion Conference and Exhibit, AIAA-2000-3242.

[2] Papila, N., Shyy, W., Griffin, L., and Dorney, D. J., 2002. "Shape Optimization of Supersonic Turbines Using Global Approximation Methods". *J. Propulsion and Power*, **18**, pp. 509–518.

[3] Madsen, J. I., Shyy, W., and Haftka, R. T., 2000. "Response Surface Techniques for Diffuser Shape Optimization". *AIAA Journal*, **38**, pp. 1512–1518.

[4] Unal, R., Lepsch, R. A., and McMillin, M. L., September, 1998. "Response Surface Model Building and Multidisciplinary Optimization Using D-optimal Designs". 7th AIAA/USAF/NASA/ISSMO Symposium on Multidisciplinary Analysis and Optimization, AIAA-1998-4759.

[5] Myers, R. H., and Montgomery, D. C., 2002. *Response Surface Methodology*, 2nd ed. John Wiley & Sons, Inc. ISBN 0-471-41255-4.

[6] Burman, J., 2003. "Geometry Parameterisation and Response Surface-Based Shape Optimisation of Aero-Engine Compressors". PhD thesis, Department of Applied Physics and Mechanical Engineering, Luleå University of Technology, Luleå.

[7] Eriksson, L.-E., 1995. Development and Validation of Highly Modular Flow Solver Versions in G2DFLOW and G3DFLOW. Internal report 9970-1162, Volvo Aero Corporation, Sweden.

[8] Wilcox, D. C., 1998. *Turbulence Modeling for CFD*, 2nd ed. DCW Industries Inc. ISBN 0-9636051-5-1.

[9] Chien, K. Y., 1982. "Predictions of Channel and Boundary-layer Flows With a Low-Reynolds-number Turbulence Model". *AIAA Journal*, **20**, pp. 33–38.

[10] Boggs, P. T., and Tolle, J. W., 1995. "Sequential Quadratic Programming". In *Acta Numerica*. pp. 1–51.

[11] Arroyo, C., Axelsson, L.-U., Håll, U., Johansson, T. G., Larsson, J., and Haselbach, F. "Large Scale Low Speed Facility for Investigating Intermediate Turbine Duct Flows". 44th AIAA Aerospace Sciences Meeting and Exhibit, AIAA-2006-1312.

[12] Sovran, G., and Klomp, E. D., 1967. *Experimentally Determined Optimum Geometries for Rectlinear Diffusers with Rectangular, Conical or Annular Cross-section*, G. Sovran ed. Fluid Mechanics of Internal Flow, Elsevier Publishing Co.